Design rules for pumping and metering of highly viscous fluids in microfluidics†

Sarah L. Perry, Jonathan J. L. Higdon and Paul J. A. Kenis*

Received 18th May 2010, Accepted 26th August 2010
DOI: 10.1039/c0lc00035c

The use of fluids that are significantly more viscous than water in microfluidics has been limited due to their high resistance to flow in microscale channels. This paper reports a theoretical treatment for the flow of highly viscous fluids in deforming microfluidic channels, particularly with respect to transient effects, and discusses the implications of these effects on the design of appropriate microfluidic devices for highly viscous fluids. We couple theory describing flow in a deforming channel with design equations, both for steady-state flows and for the transient periods associated with the initial deformation and final relaxation of a channel. The results of this analysis allow us to describe these systems and also to assess the significance of different parameters on various deformation and/or transient effects. To exemplify their utility, we apply these design rules to two applications: (i) pumping highly viscous fluids for a nanolitre scale mixing application and (ii) precise metering of fluids in microfluidics.

1. Introduction

Microfluidic approaches have been demonstrated for a wide variety of applications ranging from virus detection[1] and protein crystallization[2] to distillation[3] and fuel cells.[4] The idea of a "lab on a chip," capable of performing ever more complex chemical and/or biological processes, has been realized in numerous examples through the integration of multiple unit operations such as mixing, reaction, separation, and detection on a single chip. Soft lithography continues to spur the development of microfluidic technology by providing a fast and easy method for the rapid prototyping of highly complex networks of channels with integrated pneumatic valves and peristaltic pumps.[5] The elastomer polydimethylsiloxane (PDMS) has been used in particular for this purpose because of its ability to replicate features down to sub-micrometre length scales, such as photolithographically defined channel networks, and the ease by which the resulting molded layers can be assembled into fully functional microfluidic chips.[6] Additional advantages of PDMS over other materials include its optical transparency and its elasticity. The bulk properties of PDMS are equivalent to an incompressible rubber-like elastic material, with a Young's modulus E typically in the range of 0.5 to 4 MPa and a Poisson ratio of $\sigma = 0.5$.[7,8] The pneumatic valves and peristaltic pumps that are now being used in many microfluidic devices would not be possible without the high level of deformability of PDMS.[9–11] A number of models for these pneumatic valves and pumps have been reported to describe and predict their operation.[12–14]

To date microfluidic applications have been mostly limited to systems where the fluid viscosities are similar to that of water because of the challenges associated with pumping highly viscous and/or non-Newtonian flows. In fact, the pressures that would be required to drive highly viscous fluids (*i.e.*, $\sim 10^5\times$ more viscous than water) through a typical microfluidic channel can be extreme, to the point of exceeding the ability of most pumping systems used for microfluidics, and/or the capacity of the materials to sustain such high pressures.[15–17] Thus, strategies that overcome these challenges are needed to enable the pumping of viscous fluids. In designing a microfluidic device for use with highly viscous fluids, the single most important consideration is the viscous resistance to flow. Microfluidic devices are typically operated under conditions of low Reynolds number flow. Steady-state operation at low Reynolds number requires $\rho uh/\eta \ll 1$ while for unsteady flow we have the additional requirement that $\rho\omega h/\eta \ll 1$, where ρ is the fluid density, u is the linear flow velocity, h is the channel height, η is the fluid viscosity, and ω is the frequency of oscillation. For the laminar flows encountered in microfluidic devices, resistance to flow scales linearly with viscosity and the length of a channel and with the inverse square of the cross-sectional area of a channel.[18] Thus for a specified maximum pressure, flow resistance can be decreased by decreasing the length over which the fluid is flowing, and especially by enlarging the cross-sectional area of the channel. While these geometric modifications can be used to facilitate flow of viscous fluids, the pressures required for flow in a given microfluidic configuration may cause the microfluidic channels to deform, particularly if elastomeric materials such as PDMS are used. Channel deformation occurs if the applied pressure exceeds the stiffness of the material. Channel geometry will vary as a function of pressure, which in turn varies as a function of position along the channel. Deformation will be larger at the inlet of the channel where the pressure is highest, and will decrease towards the outlet. Previous studies have discussed the effects of channel deformation in microfluidic configurations, but these

University of Illinois at Urbana-Champaign, Department of Chemical & Biomolecular Engineering, Urbana, IL, 61801, USA. E-mail: kenis@illinois.edu; Fax: +1 (217)333-5052; Tel: +1 (217)265-0523

† Electronic supplementary information (ESI) available: Example calculations of β for a variety of common microfluidic geometries as well as details of the curve fitting for the steady-state lag volume. See DOI: 10.1039/c0lc00035c

studies were limited to externally driven, steady-state flow.[7,19,20] Channel deformation has also been useful experimentally. Hardy *et al.* developed a microfluidic analog for the study of blood vessels by exploiting the deformability of microchannels in PDMS.[19] Channel deformation as a result of viscous fluid flow in non-rigid channels also introduces a variety of transient phenomena that may have a profound effect on the operations performed on-chip, such as the precise metering of fluids which is required in many microfluidic applications. For these and several other on-chip operations, transients as a result of viscous fluid flow must be taken into account, yet mathematical descriptions to estimate these transients are presently not available.

This paper develops relevant theory for the flow of highly viscous fluids in deforming microfluidic channels, particularly with respect to transient effects, and discusses potential implications on the design of appropriate microfluidic devices for such highly viscous fluids. A simple model for a pneumatic valve will be introduced to characterize the efficiency whereby an applied valve actuation pressure is translated into a driving force for fluid flow, and scaling relationships between valve actuation and flow effects will be identified to aid the design of microfluidic chips for viscous flows. Next the effects of channel deformation on viscous flows will be considered. After a steady-state analysis similar to prior work,[7,19,20] relevant theory will be derived for the fully transient problem. The results of the theoretical analysis will then be applied to (i) the challenges of pumping and precise metering of viscous fluids despite channel deformation effects, and (ii) the design of a microfluidic device for the mixing of highly viscous and non-Newtonian fluids.

2. Theory

2.1 The effect of valve membrane actuation on pressure-driven flow in a rigid channel

The use of integrated microfluidic pneumatic pumps, comprised of three peristaltic valves in series,[2,9,11] has become increasingly common, particularly in highly complex microfluidic networks. This kind of on-chip method to drive fluid flow is desirable because it enables complex fluid routing while providing better precision and flexibility than external pressure sources. In a multilayer microfluidic device, a valve can be defined by an area where a microfluidic feature from one layer overlaps with that of a second layer, either above or below. A thin membrane of elastomeric material separates these two layers and deflects upon the application of pressure to the valve layer, translating an externally applied pressure to an internally applied pressure *via* deflection of the membrane and eventually sealing off flow in the fluid layer (Fig. 1a). An on-chip pump can be created by placing three or more of these valves in series and actuating them in a sequence to create a peristaltic pumping action (Fig. 1b).[9]

We use a linearized model valid for small deflection of a thin membrane to elucidate the effects of various design parameters on the operation of these valves and the resultant downstream pressure on the fluid.[21] More accurate predictions may be obtained through detailed non-linear analyses,[12–14] however, the linear model captures the essential scaling needed for the design of microfluidic valves. For the case of a circular membrane, the pressure drop associated with this deflection is described by

$$P_{\mathrm{appl}} - P_{\mathrm{in}} = \frac{16Ea^3z}{3(1-\sigma^2)s^4} \quad (1)$$

where the Young's modulus E and Poisson's ratio σ characterize the deformability of the valve material, and the valve membrane is of radius s, thickness a, and experiences an applied pressure P_{appl} (Fig. 1d). Deflection of the membrane is taken to be in the z-direction and is characteristic of the amount of deflection of the center of the membrane. We assume the valve to be fully actuated at $z = h_{\mathrm{v}}$, the height of the valve chamber. Within the valve chamber, we assume that the only pressure losses are those due to deflection of the membrane, resulting in a pressure in the valve chamber of P_{in}.

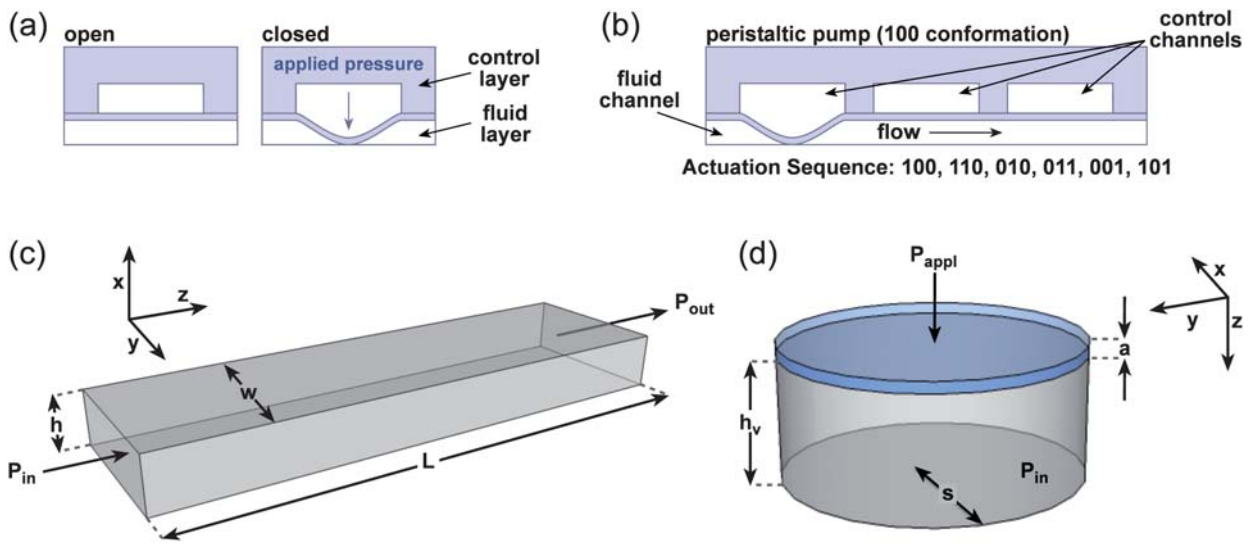

Fig. 1 (a) Depiction of the actuation of a push-down type pneumatic valve. (b) Depiction of a 3-phase peristaltic pump where a set of three pneumatic valves are actuated in sequence to drive fluid flow. The (100) actuation phase is shown. (c) Schematic depiction of a microfluidic channel of length L, width w, and height h. Inlet pressure is P_{in} and pressure at outlet is P_{out}. (d) Depiction of a theoretical pneumatic valve with circular membrane (highlighted in blue) of radius s and thickness a to be deflected a distance h_{v}. Applied pressure is P_{appl} and pressure inside of the valve is P_{in}.

We can use eqn (1) to consider the pressure driving force available for pumping after valve actuation, assuming a pressure difference across the valve of $\Delta P = P_{appl} - P_{in}$. We can then normalize eqn (1) by the applied pressure P_{appl} and define a parameter α that describes the pressure losses associated with the actuation, or stiffness, of the valve.

$$\alpha = \frac{P_{appl} - P_{in}}{P_{appl}} = \frac{16Ea^3h_v}{3P_{appl}(1-\sigma^2)s^4} \quad (2)$$

From eqn (2) it follows that the term α approaches zero when the pressure losses due to the valve are small. We can thus define the case where actuation of a pneumatic valve has a negligible effect on the pressures associated with fluid flow in the limit of $\alpha \to 0$. This limit can be approached physically by modifying the stiffness (E/P_{appl}) and/or the geometry (a^3h_v/s^4) of the valve. When the ratio of E/P_{appl} is small, the applied pressure is able to easily overcome the resistance of the valve material to deformation. The thickness of the valve membrane a along with the extent of deflection h_v can be modified along with the radius of the valve s in order to minimize the geometric term a^3h_v/s^4.

We now have a method to determine P_{in}, the pressure available for pumping at the inlet of a microfluidic channel, whether it is directly applied by an external source or determined using eqn (1). Let us now consider fluid flow in a long microfluidic channel of length L, width w, and height h (Fig. 1c). Typically microfluidic channels have a low aspect ratio such that $w \gg h$, and the channel can be treated effectively as an infinite slit. Furthermore, the small dimensions of these channels lead to a small Reynolds number and thus laminar flow. The driving pressure P_{in} is dissipated over the length of the channel to an outlet pressure of P_{out}. The z-axis is taken to be in the direction of flow along the length of the channel.

The hydrodynamics of viscous flow in an infinite slit of rigid geometry are well understood and an expression for the volumetric flow rate $\dot{V}$ can be easily derived in terms of the channel dimensions, pressure gradient dP/dz, and fluid viscosity η.[18]

$$\dot{V} = -\frac{h^3w}{12\eta}\frac{dP}{dz} \quad (3)$$

For a channel of set dimensions, which we term as a 'rigid' channel, a linear pressure drop ($\Delta P/L$) is realized over the length of the channel with $\Delta P = P_{in} - P_{out}$. Note that since the pressure front is assumed to transfer instantaneously through an incompressible fluid, our result is valid for all times.

2.2 The effect of channel deformation on viscous flow

In using elastomeric materials, deformation of the bulk material defining a channel is possible. Thus, rather than considering a thin membrane as in Section 2.1, we now consider deformation of an infinite slab subject to an applied surface pressure.

2.2.1 Steady-state viscous flow in a deformed channel. Deformation of the channel can be modeled as a distributed pressure over an infinite slab.[22] For a typical PDMS device on a stiff glass substrate, it is only necessary to consider deformation of the top wall of the microfluidic channel so long as the aspect ratio of the device does not approach unity (also a requirement for viscous flow in an infinite slit).[7,22] The maximum deformation of a slab can be written in terms of the ratio of pressure to Young's modulus P/E, a characteristic length which for a low aspect ratio channel is the width w, and a proportionality constant c which takes into consideration the geometry of the deforming area and is of order of magnitude $\sim$1.[7,19,22] Thus,

$$\Delta h_{max} = \frac{cPw(1+\sigma)}{E} \quad (4)$$

Previous work has demonstrated that this deformation is parabolic across the width of a microfluidic channel.[7,19] Owing to the nonlinear dependence on h in eqn (3), the change in $\dot{V}$ with variable h cannot be captured by using an average value for h. Nonetheless, it is convenient to compute $\langle \Delta h \rangle = 2/3\Delta h_{max}$, as has been done previously,[7,19] and thus we can write an expression for an effective height $h(z)$ along the length of the channel as a function of $P(z)$ and the initial channel height h_0. We note that the relevant coefficient for the effective height may differ from 2/3 in practice.

$$h(z) = h_0\left(1 + \frac{2cP(z)w(1+\sigma)}{3Eh_0}\right) \quad (5)$$

Substituting this function for the channel height into our expression for volumetric flow rate from eqn (3), we generate the following expression for the volumetric flow rate in a deformed channel as a function of the pressure drop along the length of the channel.

$$\dot{V} = -\frac{h_0^3w}{12\eta}\left(1 + \frac{2cPw(1+\sigma)}{3Eh_0}\right)^3\frac{\partial P}{\partial z} \quad (6)$$

At steady-state the volumetric flow rate is constant, and we can integrate eqn (6) over the length of the channel assuming an inlet pressure of P_{in} and letting $P_{out} = 0$. Combining the integrated form of eqn (6) with eqn (3) and defining a non-dimensional parameter β which characterizes the tendency of a channel to deform, we obtain an analytical form of the steady-state volumetric flow rate for a deformed channel in terms of the volumetric flow rate for a rigid channel and a correction term that depends on β. The rigid solution can be obtained by setting $\beta = 0$.

$$\dot{V}_{ssdef} = \dot{V}_{rigid}\left(1 + \frac{3\beta}{2} + \beta^2 + \frac{\beta^3}{4}\right) \quad (7)$$

where

$$\beta = \frac{2cP_{in}w(1+\sigma)}{3Eh_0} = \frac{2\Delta h_{max}}{h_0} \quad (8)$$

β describes the tendency of the material to deform given the ratio P_{in}/E. The larger the applied pressure compared to the Young's modulus, the larger the deformation. For the purposes of the analyses presented here—particularly given the approximation of flow in an infinite slit—we will only examine behavior over the range of $\beta < 3$. We established this threshold for our analysis based on the aspect ratio of the deformed device such that the assumption of an infinite slit is still valid. For example, if we consider a channel of width $w = 100$ μm and initial height $h_0 = 10$ μm our initial aspect ratio is 0.1, indicating an order of magnitude difference between the two dimensions. However, for the

case of $\beta = 3$, channel deformation results in an average channel height of $h = 40$ μm and an aspect ratio of 0.4, indicating that the height and width of the channel are of nearly the same order.

To obtain an expression for $P(z)$ we integrate eqn (6) and substitute eqn (7):

$$P(z) = \frac{P_{in}}{\beta}\left\{\left[\frac{z}{L}\left[1-(1+\beta)^4\right]+(1+\beta)^4\right]^{1/4}-1\right\} \quad (9)$$

Owing to the deformation of the channel, we see a 4th root decay of pressure along the channel length rather than the linear dependence seen in the rigid case (Fig. 2a). In the limit of small β, eqn (9) reduces to the rigid limit described by eqn (3).

Combining the expressions for channel height in eqn (5) and pressure in eqn (9), we may integrate over the length of the channel to find the change in volume V_{swell} due to the deformation.

$$V_{swell} = V_{rigid}\left[\frac{4}{5}\left(\frac{1-(1+\beta)^5}{1-(1+\beta)^4}\right)-1\right] \quad (10)$$

Having developed the mathematics behind steady-state flow in a deformed channel, let us examine the physical meaning behind some of these results. As described in eqn (9), and shown in Fig. 2a, the pressure profile along the length of the channel is nonlinear, which corresponds to the channel deformation. At the beginning of the channel where the large applied pressure results in a large deformation, relatively small pressure losses occur resulting in pressure gradients that are lower than for the purely rigid case.

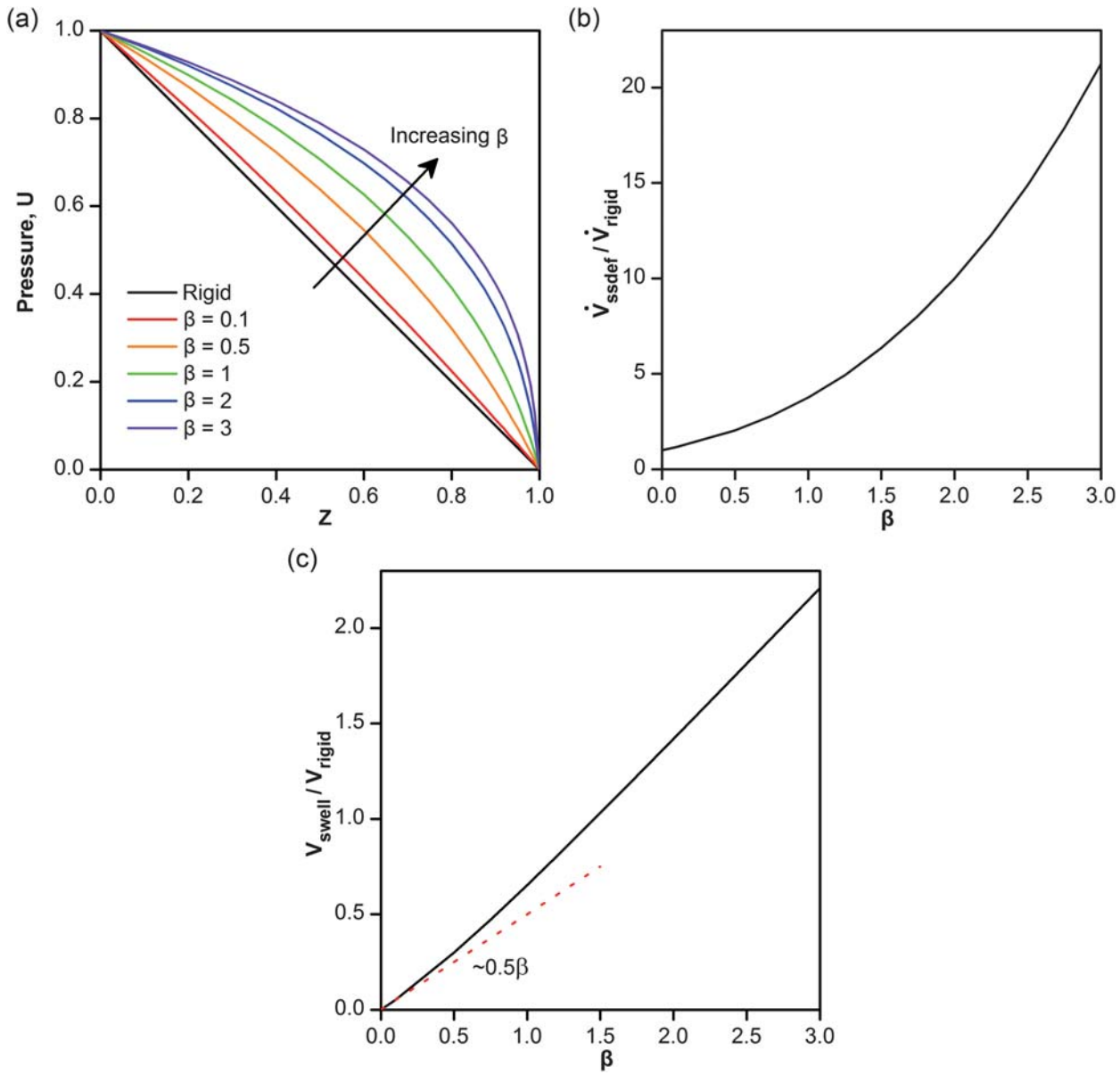

Fig. 2 Plots of (a) steady-state pressure profiles for different values of β along the microfluidic channel. Pressures in the deformed channels are larger than the linear rigid case at all points in the channel. (b) Steady-state volumetric flow rate normalized by the flow rate in a rigid channel as a function of the deformation parameter β. (c) The change in the channel volume normalized by the rigid channel volume as a function of β. In the limit of small β this curve can be approximated as 0.5β, as shown.

However, near the end of the channel where deformations are small, we observe much steeper pressure gradients. Both channel deformation and steeper pressure gradients combine to enhance the volumetric flow rate. At steady-state, the most significant result of channel deformation is the 3rd order polynomial dependence of the volumetric flow rate on β described in eqn (7) and plotted in Fig. 2b. While for small deformations this effect can be neglected, a dramatic increase in flow rates is seen at larger deformations. For example, at a value of $\beta = 1$, typical for many microfluidic systems, the volumetric flow rate resulting from the deformed channel is 375% higher than the corresponding flow rate expected for a rigid channel. (See the ESI† for calculated values of β as a function of various microfluidic device geometries.) An additional effect of channel deformation is an increase in the total volume of the channel. While the precise dependence of the swell volume with respect to deformation given in eqn (10) is complicated, one can approximate the relationship depicted in Fig. 2c as $V_{swell}/V_{rigid} \approx 0.5\beta$ from a Taylor series expansion for small β. The effect of the swell volume should have little impact on steady-state operation of a device but can become significant when considering unsteady effects where the channel volume changes with time, causing the inlet and outlet volumetric flow rates to be unequal.

2.2.2 Unsteady viscous flow in a deforming channel. To examine unsteady viscous flow, we begin with a mass balance relating changes in h to $\dot{V}$.

$$\frac{\partial h}{\partial t} = -\frac{1}{w}\frac{\partial \dot{V}}{\partial z} \tag{11}$$

Assuming that h changes slowly with z, we can combine eqn (11) with the expression for volumetric flow rate, eqn (6), and write an equation for the channel pressure P as a function of z and t.

$$\frac{\partial P}{\partial t} = \frac{\partial}{\partial z}\left[\frac{Eh_0^3}{8c\eta w(1+\sigma)}\left(1+\frac{2cPw(1+\sigma)}{3Eh_0}\right)^3\frac{\partial P}{\partial z}\right] \tag{12}$$

The initial condition is $P = 0$ at $t = 0$, and boundary conditions are $P = P_{in}$ at $z = 0$; $P = 0$ at $z = L$.

The expression is non-dimensionalized using the core variables: applied pressure P_{in}, the channel length L, and the fluid viscosity η. These variables are chosen because they are physical parameters which can be easily controlled and which define resultant quantities in our system such as volumetric flow rate. The non-dimensional forms of the variables are:

$$U = \frac{P}{P_{in}}, \quad Z = \frac{z}{L}, \quad \tau = \frac{tP_{in}}{\eta} \tag{13}$$

Applying this non-dimensionalization and the definition for β from eqn (8), we obtain the partial differential equation:

$$\frac{\partial U}{\partial \tau} = \frac{\partial}{\partial Z}\left[\gamma(1+\beta U)^3\frac{\partial U}{\partial Z}\right] \tag{14}$$

The non-dimensionalized initial condition is $U = 0$ at $\tau = 0$, the boundary conditions are $U = 1$ at $Z = 0$; $U = 0$ at $Z = 1$, and γ is defined as:

$$\gamma = \frac{1}{12\beta}\left(\frac{h_0}{L}\right)^2 \tag{15}$$

The form of eqn (14) is analogous to that of a diffusion equation with a variable diffusivity of $\gamma(1 + \beta U)^3$.

Because γ is related to this variable diffusivity we can use it to define a dimensionless diffusive time τ^*.

$$\tau^* = \gamma\tau = \frac{\gamma P_{in} t}{\eta} \tag{16}$$

With this definition we obtain the modified partial differential equation:

$$\frac{\partial U}{\partial \tau^*} = \frac{\partial}{\partial Z}\left[(1+\beta U)^3\frac{\partial U}{\partial Z}\right] \tag{17}$$

The modified non-dimensionalized initial condition is $U = 0$ at $\tau^* = 0$, and the boundary conditions are $U = 1$ at $Z = 0$; $U = 0$ at $Z = 1$.

The boundary value problem defined by eqn (17) with associated initial and boundary conditions was solved numerically in MATLAB (Mathworks Inc., version 7.6.0.324).[23] A variable grid mesh was used to capture the increasingly steep behavior of the function near the outlet at $Z = 1$. At long times the solution is observed to approach the steady-state values predicted from the analytical solutions. Results are shown below for $\beta = 1$, which is typical for a PDMS channel (Fig. 3).

As mentioned previously, the form of the boundary value problem is the same as nonlinear diffusion in a channel. It is intuitive to think of a large slug of concentration entering the channel and then slowly diffusing along its length. In an analogous fashion, the pressure profile within the channel develops first as a sharp impulse at the entrance of the channel and then spreads down the length of the channel as deformation occurs and steady-state is reached (Fig. 3a). From eqn (5) the channel height scales directly with pressure. Deformation or "inflation" of the channel due to the applied pressures thus matches the changes in pressure profile.

The initial impulse of pressure also translates to the initial generation of steep pressure gradients. These steep gradients allow for rapid filling at the start of the deforming channel. However, the pressure gradients take time to propagate down the length of the channel, resulting in a lag between the start of flow at the inlet and the observation of flow at the outlet. This lag time can be more clearly observed by examining a plot of normalized volumetric flow rate at the outlet as a function of time (Fig. 3c).

A similar analysis can be used to examine the case where a deformed channel is allowed to relax in the absence of an inlet pressure. In this instance the pressure driving force for flow comes from the deformed channel as it relaxes. Referring again to the diffusion analogy, the steady-state concentration (or in our case pressure) profile slowly decays to zero as material diffuses to the outlet (Fig. 3b). However, the driving force for this diffusion decreases with time as the concentration profile levels out in the channel. Translating this analogy to pressure and fluid flow, we observe an initially high flow rate at the outlet that asymptotically approaches zero as the pressure gradients in the channel become negligible (Fig. 3c).

The trends in the pressure driving force for flow are very different between the filling and emptying cases. For the filling case there is a constant inlet pressure that then propagates along the length of the channel. This results in a fairly rapid approach to steady-state. However, for the emptying case the pressure driving force decreases with time, asymptotically approaching

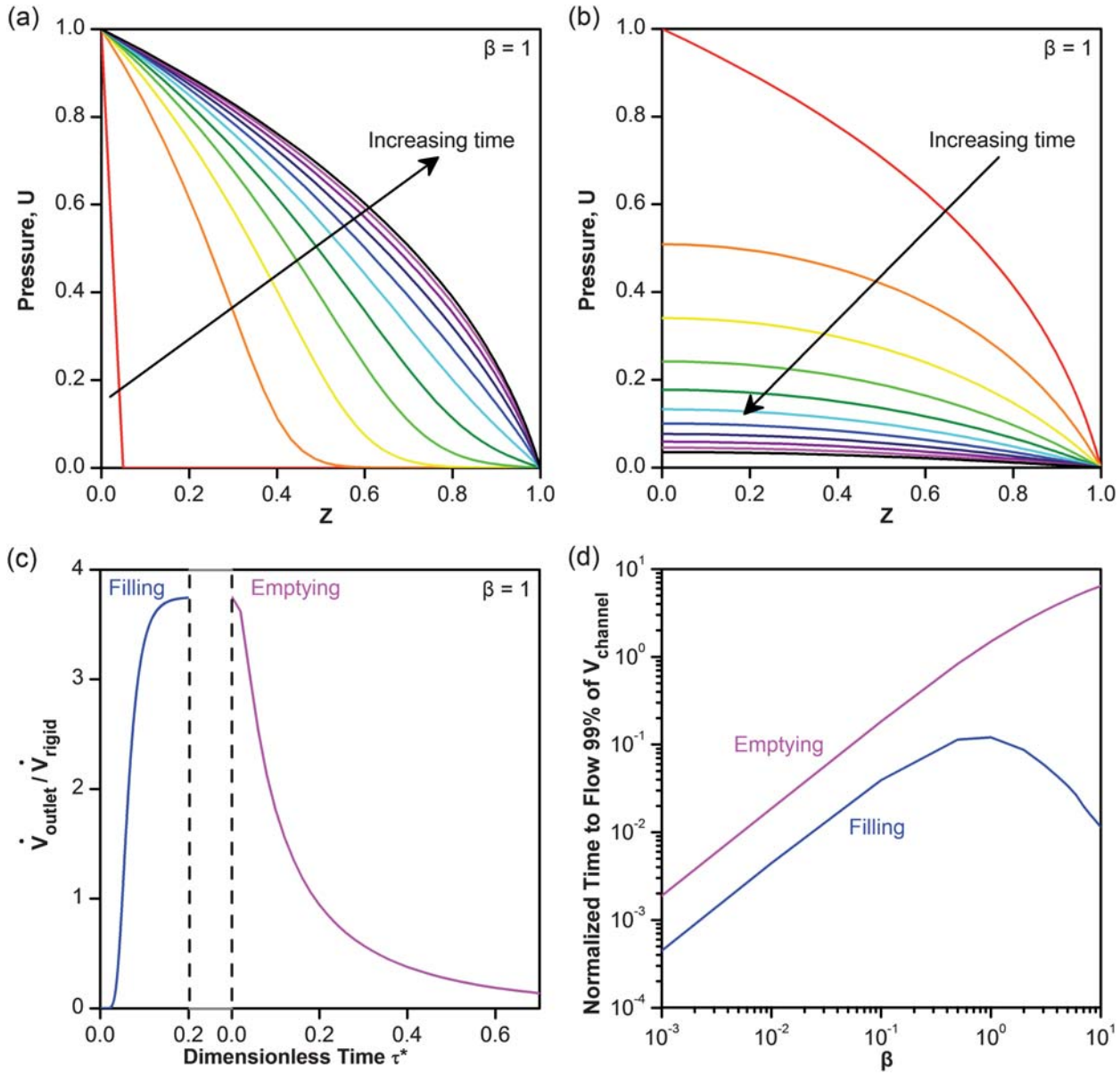

Fig. 3 Results from the MATLAB simulation of the fully transient problem of pressure-driven viscous flow in a deforming channel using parameters that are typical for flow in a PDMS channel giving a value of $\beta = 1$. Here the channel is deforming to reach a steady-state profile over time. (a) Dimensionless pressure over the length of the channel Z at intervals from $\tau^* = 0$ to $\tau^* = 0.1$ for the filling case, and (b) over intervals from $\tau^* = 0$ to $\tau^* = 1.0$ for the emptying case. (c) Volumetric flow rate at the outlet normalized by the flow rate for a rigid channel as a function of time for both filling and emptying. (d) Time to fill or empty 99% of the channel volume for the transient filling and emptying cases, respectively, as normalized to the rigid case.

zero. A comparison of the outlet volumetric flow rate curves for the two cases in Fig. 3c shows that the time to reach steady-state is significantly longer for the emptying case.

We can also examine how the rate at which a deforming channel approaches steady-state varies with β (Fig. 3d). We characterize the time for filling as the swell volume divided by the volumetric flow rate. If we then analyze the β dependence of this filling time we obtain the result:

$$t_{fill} \approx \frac{V_{swell}}{\dot{V}} \approx \frac{\beta P}{(1+\beta P)^3} \tag{18}$$

In the limit of small β, the filling time scales linearly with β. This relationship is the result of roughly linear increases in the swell volume that dominates over negligible increases in the volumetric flow rate. However, in the limit of large β, the time scales as the inverse square of β as increases in the channel volume are balanced by the geometric increases in the volumetric flow rate.

While it is more difficult to extract trends for the emptying case, Fig. 3c and d clearly show that the time for the emptying case to reach steady-state is significantly longer than that of the filling case. Despite this difference, similar trends with β are observed.

3. Design rules

In Section 2 a theoretical analysis of various aspects of the microfluidic system yielded key equations to describe flow in

rigid and deforming channels as well as the ability to induce pressure-driven flow by the actuation of microfluidic pneumatic valves. Here we will analyze these key equations to establish practical design rules for use in the design of microfluidic devices. We will first summarize the effects of pneumatic valves on pressure-driven flow (Section 3.1). We will then consider the case of steady-state pumping in a channel, including the possible effects of channel deformation (Section 3.2). Next we focus on metering applications and present three different strategies to achieve precise metering while accounting for both steady-state and transient channel deformation effects (Section 3.3). In Section 3.4 we will apply these design rules to two cases in actual microfluidic applications.

Note that the expressions given here reflect only the scaling behavior of the various parameters. For applications where high precision is required, the values predicted here may not be sufficiently accurate. In those cases, the device should either be calibrated under actual operating conditions or the theory should be modified to more accurately describe such cases.

3.1 Effective pneumatic valves for pumping viscous fluids

In this paper we are concerned with the idea of handling viscous fluids in a microfluidic device. Overcoming the resistance of highly viscous fluids typically necessitates a high pressure driving force. Therefore, it is important to minimize ancillary pressure losses associated with the transfer of pressure to the fluid, as with the actuation of a pneumatic valve.

In eqn (2) we established a parameter α which describes pressure losses associated with stiffness during the actuation of the valve. This gives us a design equation for the effective incorporation of microfluidic pneumatic valves to drive fluid flow. In the limit of an ideal valve that actuates without pressure losses the parameter $\alpha \rightarrow 0$. In designing a valve for pumping, we can optimize the parameters in eqn (2) corresponding to the geometry (a^3h_v/s^4) and the relative stiffness of the valve (E/P_{appl}) to minimize the value of α.

Using typical physical constants for PDMS ($E = 700$ kPa and $\sigma = 0.5$)[7,8] and typical valve configurations ($a = 10$ μm and $h_v = 10$ μm), the value of α is small (<0.05) for valve sizes $s > 100$ μm at actuation pressures as low as 10 kPa (1.45 psi). Similar values for α can be obtained with smaller valves through the use of higher pressures.

The results presented here are similar to work done by Quake *et al.* concerning the design of a valve.[12] While the goal of their work was the creation of a valve that could be actuated successfully, here we extend their ideas to design a valve with minimal pressure losses.

The simplest pumping scenario is the constant pressure case where steady-state can be reached and maintained. This can be achieved through the use of an external syringe pump or pressure source. However, on-chip pumping by a series of pneumatic valves is inherently a discrete process which can be characterized as a fluctuating pressure source. As shown in Fig. 1b, a pneumatic pump can be created by arranging three or more valves in series, and actuating these valves in a peristaltic sequence (100, 110, 010, 011, 001, and 101 where 1 refers to the actuation or closing of a valve and 0 refers to the opening of a particular valve in the series).[9] Thus, six sequential valve actuations must take place for a discrete unit of fluid to be pushed through the pump. For such a pump to maintain a pseudo-steady-state flow in a deformed channel, the timescale of the pumping cycles must be smaller than the timescale for relaxation of the deformed channel. However, the timescale for pumping must also be longer than the timescale for relaxation of the small segments of deforming channel between valves. Fortunately, the distance between pump valves is typically small and since the relaxation time scales with channel length, the relaxation time for these small channel segments is not significant.

While balancing pump design against deformation of the channel may need to be considered in extreme cases, the advantage of moving fluid within a peristaltic pump as opposed to down a long channel is the difference in length-scale. The distance between sequential valves in a pump can be made very short, allowing for a high driving force. Flow between valves can be further facilitated by considering the dimensions of the valves as compared to the fluid channel as per eqn (3). Increasing the width or height of the valve allows for easier flow. In fact, if the design rules associated with Section 3.1 and eqn (2) have been used to design an efficient valve, the thin membrane forming the "roof" of each of the valves can be allowed to deflect upwards, providing an artificially larger chamber for the fluid to enter.

3.2 Steady-state pumping in a microfluidic channel

Eqn (3) provides us with a design equation where we can optimize parameters such as the applied pressure, flow rate, and channel geometry in order to facilitate the flow of a fixed volume of a viscous fluid. Using an initial channel design and specifying a volumetric flow rate, we can first estimate the applied pressure that would be needed to drive flow and then adjust the design and/or operation of the device to lower this pressure if it is not feasible.

However, while large applied pressures can be used to drive flow, such increases also affect the potential for channel deformation to occur. Thus we have examined the combined effects of changing a particular parameter first on the pressure using eqn (3), and then the total effect of both the parameter and the pressure change on β using eqn (8). As an example, consider the parameter h. The pressure scales as $1/h^3$ and β scales as $\Delta P/h$, thus the total effect is $\beta \approx 1/h^4$. The scaling of these parameters is given in Table 1.

Table 1 provides a 1st order estimate of the scaling relationships that various geometric, materials, and operational parameters have on the applied pressure necessary to drive flow and on the resultant deformation. For small deformations ($\beta \ll 1$), these scaling relationships constitute a rigorous quantitative estimate. For $\beta \approx 1$, these estimates may be refined to give quantitative predictions using eqn (7), the full expression for volumetric flow in a deformed channel. It is interesting to note that for the same initial microfluidic geometry (identical w, h, and L) and fluid, a larger extent of channel deformation (*i.e.* lower E) will result in a higher steady-state volumetric flow rate for a given applied pressure. Thus while analysis of the resultant system is more complicated, the deformation itself could be beneficial.

3.3 Precise metering operations

In many microfluidic applications it is necessary not only to pump fluids but to do so with precise control over the volumes

Table 1 Scaling relationships for steady-state pumping of a fixed volume of a viscous fluid developed from eqn (3) and (8)

Parameter	Flow effect	Deformation effect
w	$\Delta P \approx 1/w$	$\beta \approx$ constant
h	$\Delta P \approx 1/h^3$	$\beta \approx 1/h^4$
L	$\Delta P \approx L$	$\beta \approx L$
t	$\Delta P \approx 1/t$	$\beta \approx 1/t$
E	No effect	$\beta \approx 1/E$

metered. Pumping fluids in a rigid channel is simple because flow achieves steady-state instantaneously. Thus the simplest strategy to design a device for precise metering is to use the scaling relationships in Table 1 such that β is small and deformations can be neglected. If design of a microfluidic device such that channel deformation is negligible is not possible, it becomes necessary to carefully account for transient periods associated with the starting and stopping of flow. Here we present three strategies for precise metering in a deformed channel which balance the speed of a single metering operation against simplicity of operation.

3.3.1 Steady-state metering with a shunt. For flow in a deforming channel, transient effects are associated only with the initial filling of the channel before steady-state is reached, and the relaxation of the channel once the applied pressure is removed. While the behavior of these transient periods can be accounted for, the device design and operation can be modified to decouple these transient periods from the actual metering operation by establishing a shunt to which flow can be directed during these transient periods or between metering instances. In this manner, steady-state flow as predicted by eqn (7) can be established in the channel, and then flow can be switched from the shunt to the desired outlet as needed.

This method can provide very fast metering but requires more complicated control over the various flow streams. Additionally, it is potentially wasteful with respect to the material shunted.

3.3.2 Metering with an initial transient (half-shunt). To avoid the complications of switching between shunting and metering operations while maintaining steady-state, we could instead account for the initial transient behavior while using a shunt to avoid the transient associated with channel relaxation. We begin with a fully relaxed channel and the fluid at rest. During metering we observe a lag between the start of pumping and the evolution of flow at the outlet which can be treated as a correction to the steady-state solution. Once the desired quantity of fluid has been metered we can simply seal the outlet of the channel to prevent excess fluid associated with the channel deformation from affecting the precision of our metering. The excess fluid present in the deformed channel can then be drained away as the channel returns to its rest state.

Let us define a correction in terms of a lag time or a lag volume which is the difference between the actual, or transient, curve and the volume of fluid which would be metered at steady-state (Fig. 4a). This value can then be added as a constant correction term to the steady-state solution predicted by eqn (7).

$$t_{\mathrm{lag}}(V) = t(V) - t_{\mathrm{ss}} \tag{19}$$

$$V_{\mathrm{lag}}(t) = V_{\mathrm{ss}} - V(t) \tag{20}$$

While Fig. 4a provides a graph of the lag volume for $\beta = 1$, developing a universal relationship for all values of β is more useful. Because the lag volume increases exponentially during the transient period before asymptotically leveling off at steady-state it is useful to normalize the lag volume to that of the steady-state value, V_{lagss}. The dependence of lag volume on time is more complicated. However, an effective time can be defined based on a 2nd order polynomial scaling for the dimensionless diffusive time, $\tau_{\mathrm{scale}}^* = A\tau^{*2} + B\tau^*$ allowing us to collapse the lag volume data for all β onto a universal curve which was then fit to an exponential function (Fig. 4b). Details of this scaling and correlations for the coefficients A and B as functions of β are given in the ESI†.

Examining variations of the steady-state lag time and lag volume as a function of β (Fig. 4c) is also useful. Similar to the trends observed in the swelled volume of the channel (Fig. 2c), the steady-state lag volume increases in a nearly linear fashion as a function of β. This similarity is expected since the lag volume is directly related to the extra volume of fluid needed to fill the deformed channel. Actual values for the lag time and lag volume are calculated and discussed in Section 3.4.3 below.

The trends in the relationship of lag time *vs.* β are identical to those observed for the time to fill a channel *vs.* β from eqn (18) and Fig. 3d. At small deformations a nearly linear relationship between lag time and β exists because increases in the channel volume dominate over the relatively small increases in the volumetric flow rate. However, as deformation becomes more pronounced, the benefits of an increased volumetric flow rate are counteracted by increases in channel volume, resulting in an inverse square dependence of lag time with β.

As demonstrated in Fig. 3c, the timescale for the transient period associated with filling a deforming channel is significantly shorter than the timescale associated with relaxation of the channel. Thus while the half-shunt metering strategy described here is slower than the fully steady-state shunt method (Section 3.3.1), it is faster than the fully transient strategy presented in Section 3.3.3 below.

3.3.3 Fully transient metering. The simplest method for precise metering is also the slowest and involves considering the fully transient problem. In this case the pressures associated with pumping will first cause the channel to deform. Thus the time associated with this initial transient can be estimated using the plots of lag volume (Fig. 4). If the volume to be metered is such that the system reaches steady-state, eqn (7) can be used as previously to determine the time needed for pumping. However, we must now also consider the time needed to fully relax the channel and thus empty out the desired volume of fluid. Fig. 3d provides an estimate of the time needed for the channel to fully relax as a function of β.

In determining a metering protocol for this fully transient case, the previously described strategies can be used to determine the time for the desired volume of fluid minus that of the swell volume to reach the outlet. At this point the pumping must be shut off and the inlet of the channel sealed to prevent backflow.

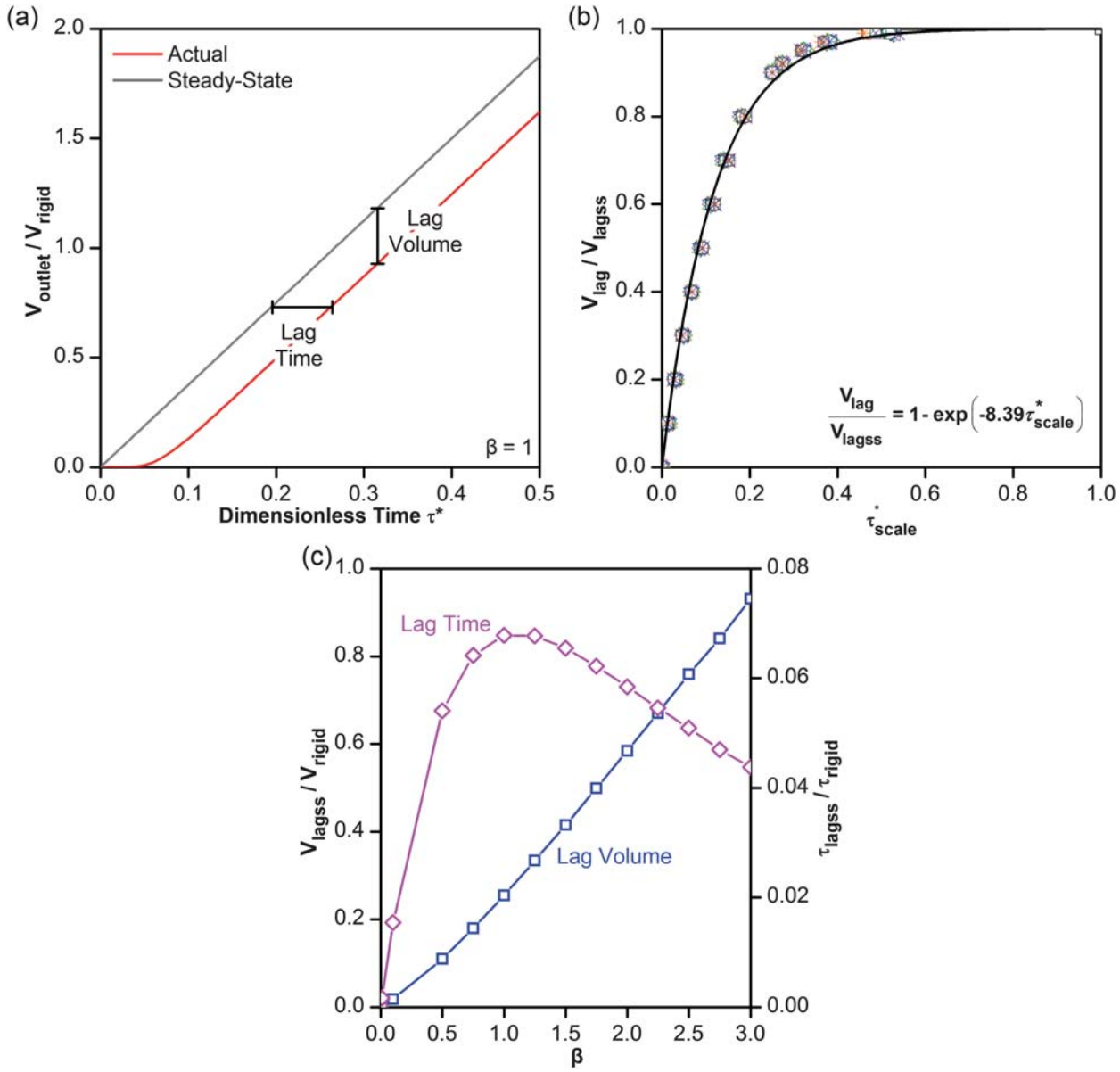

Fig. 4 Results from the MATLAB simulation of the fully transient problem of pressure-driven viscous flow in a deforming channel. (a) The volume passing through the outlet normalized by the volume of a rigid channel as a function of time for the transient case and for hypothetical instantaneous steady-state flow for $\beta = 1$. (b) A plot of normalized lag volume *vs.* a scaled dimensionless time. The solid curve is an exponential fit to the data which is universal for all β. (c) The steady-state lag time normalized by the time for flow in the rigid case to accomplish a total rigid channel volume and the steady-state lag volume normalized to the channel volume for metering as a function of β.

3.4 Applications of the design rules

Thus far we have described the physics behind various phenomena present in a microfluidic device and developed associated design rules. Let us now apply these design rules to two examples in actual microfluidic applications: (i) a microfluidic device for mixing highly viscous fluids and (ii) the precise metering of fluid using a pneumatic on-chip pump over a range of fluid viscosities.

3.4.1 Creating a mixer for highly viscous fluids. Microfluidic applications involving highly viscous fluids have lagged behind their less viscous counterparts mostly because of the difficulty in flowing high viscosity fluids on the microscale. The simple scaling relationships that resulted from the work presented above (Table 1) enable the design of microfluidic devices capable of driving flow for fluids that are not only highly viscous but also non-Newtonian. We coupled these design rules with strategies for mixing to create a microfluidic mixer capable of operating with fluids of both differing and high viscosities.[2]

The majority of microfluidic mixers, such as the ring mixer devised by the Quake group[11,24,25] or the herringbone mixer devised by Stroock and coworkers,[26,27] require driving flow over relatively long distances. These mixer designs have difficulty operating with higher viscosity fluids, especially when trying to

mix fluids of significantly different viscosities. Thus instead of striving to establish complex flow patterns in a long channel, we chose to develop a mixing strategy that is compatible with the need to pump higher viscosity fluids (Fig. 5). Previously we reported on the operation and application of this device to mix a viscous lipid (monoolein) and an inviscid aqueous solution.[2] Here we describe how the scaling relationships were used in its design. The viscous fluid mixer is composed of three microfluidic chambers connected by small microfluidic channels. In this two-layer PDMS device, isolation valves are located both over the inlet lines used to fill the device and over the channels connecting each of the three chambers. Large microfluidic injection valves are also located over each of the three large chambers containing the fluids to be mixed. These injection valves are used to pump fluid from one compartment to another while the various isolation valves on the connecting channels control the direction of fluid flow. Mixing is achieved by first driving flow in a linear fashion from the side chambers into the center chamber through all of the available injection lines. Two recirculating loops of flow are then created on the two halves of the device by using first one injection line for flow to the side chambers, then two lines to return to the center chamber, and then again a single line to refill the side chambers. These straight-line and recirculating flow patterns are repeated to drive fluid mixing in a tendril–whorl fashion.[28] We used this mixer to prepare self-assembling aqueous/lipid mesophases where the viscosity of the initial aqueous and lipid solutions differed by a factor of ~30 (2.45×10^{-2} Pa s for the lipid phase *versus* 7.98×10^{-4} Pa s for the aqueous phase). Furthermore, the resulting mixture had a viscosity ~10^5 times larger than that of water (~48.3 Pa s at a shear rate of 71.4 s^{-1}) and displayed non-Newtonian fluid behavior. These mesophases are of interest particularly in structural biology applications, including membrane protein crystallization.[29]

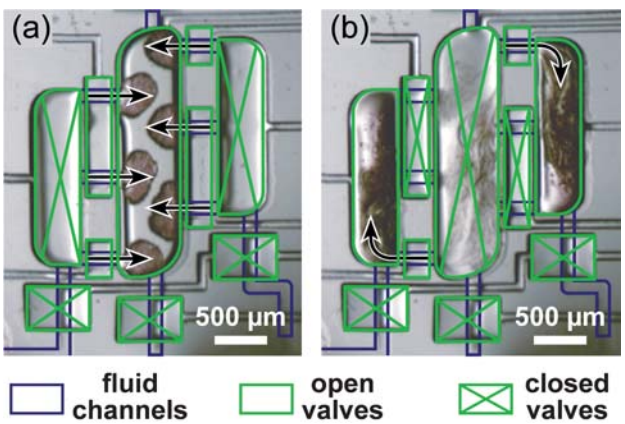

Fig. 5 Optical micrograph of a microfluidic mixer designed to mix highly viscous fluids or fluids of vastly different viscosities. Pneumatic valves are outlined in green and are located as isolation valves over inlet lines leading into each of three larger chambers as well as over lines connecting the three chambers. Valves used to drive fluid flow are located over each of the three large chambers. (a) The injection of an aqueous solution from the side chambers into the center chamber containing a highly viscous lipid. (b) Injection of fluid from the center chamber to the side chambers through a single injection line. See ref. 2 for more details on the mixing sequence.[2]

In designing this microfluidic mixing device, the first challenge that needed to be overcome was pumping fluids with viscosities several orders of magnitude higher than water. We were able to counter this increased viscous resistance by designing the geometry of our device based on the design rules in Table 1, such that operational parameters, including the applied pressure to drive flow, could be optimized (*i.e.* minimized to attainable pressure levels). Instead of trying to pump a highly viscous fluid over a long distance in a narrow channel, we configured the mixer such that (i) the distance for flow L is short and (ii) the width w of the device is large. The use of large fluid chambers allowed us to minimize the distance over which fluid was pumped in a narrow channel. These large chambers have the added benefit of ensuring, as per the scaling relationships associated with the parameter α in eqn (2), that the pneumatic valves located over each chamber are able to efficiently drive flow without significant pressure losses. Including these chamber valves in our design provided two additional benefits: (i) whereas the actual height of the fluid chambers in our device is a constant, the presence of an easily deflectable valve over each of the chambers allows us to effectively consider each of the chambers as having a much larger height than was initially designed. The design rules derived here (Table 1) show that the required pressure to drive viscous flow scales with the cube of the channel height, meaning that even small increases in height significantly decrease the pressure needed to drive fluid flow. (ii) We were able to pump the entire contents of each individual chamber with a single actuation, rather than by repeated pumping steps to move smaller portions of fluid around. (iii) Lastly, we were also able to operate our device relatively slowly such that adverse effects of the increased fluid viscosity which we had not overcome through device design could be compensated for by accepting a lower flow rate. The mesophase that is formed upon mixing in this study also displayed viscoelastic behavior. An additional benefit of the decreased flow rate was adequate compensation for the relaxation timescales associated with the fluid.

Based on the geometry of the device and the large applied pressures needed to drive flow, our calculated value of $\beta \approx 2$ indicates that deformation of the channels connecting the compartments will be significant. As discussed previously (Section 2.2), this kind of deformation decreases pressure losses along the length of a channel and can provide further benefits for moving highly viscous fluids between chambers. While deformation is only an issue for the short channels connecting the larger microfluidic chambers, the short length of these channels means that the lag time and volume will be relatively small compared to the total volume of fluid to be pumped. Additionally, relaxation of the extra volume in these channels is not a concern because microfluidic isolation valves over each of these channels are actuated as part of the mixing sequence and will expel fluid remaining in the channel.

3.4.2 Peristaltic fluid metering

The case of a rigid channel. The ability to precisely meter out picolitre-scale (or smaller) quantities of fluids has been clearly demonstrated in microfluidic devices, typically by the peristaltic actuation of a series of pneumatic valves.[24] This method typically assumes that the volume of fluid displaced under the valve will be moved down the channel without losses due to channel

deformation. For a given driving pressure ΔP, eqn (3) gives the maximum flow rate through a channel based on the channel geometry and fluid viscosity. When using a peristaltic pump we can calculate an average volumetric flow rate based on the volume displaced by a single cycle of the pump V_{valve} and the pumping frequency f.

$$\dot{V} = fV_{valve} \tag{21}$$

The pump should be capable of pumping at any flow rate up to the maximum flow rate specified by the channel geometry and fluid viscosity at which point the viscous resistance to flow will dominate over pumping rate. We can determine the associated maximum pumping frequency for a given system by combining eqn (3) and (21):

$$f = \left(\frac{h^3 w \Delta P}{12 L V_{valve}}\right)\frac{1}{\eta} = \frac{k_{system}}{\eta} \tag{22}$$

In the interest of examining viscosity effects on pumping, we can define a system parameter k_{system} which captures the geometric and operating parameters of the system as shown in eqn (22).

Hansen and coworkers describe the exact problem resulting from a limiting pump speed in their work on a microfluidic formulator.[24] In this formulator they use a three valve peristaltic pump to precisely meter out small volumes (~80 pL) of fluid. While for aqueous solutions ($\eta \approx 0.001$ Pa s) they are capable of successfully operating their pump at a very fast rate of 100 Hz, they observe a drop-off in metering accuracy for more viscous fluids ($\eta \approx 0.4$ Pa s) even at a pump rate of 10 Hz. They determined that it was necessary to decrease the pump speed to 5 Hz in order to accurately meter out the more viscous fluid.

Using the analysis provided by eqn (22) with the geometry of the microfluidic formulator used by Hansen and coworkers ($h =$ 9 μm, $w = 80$ μm, $L = 4712$ μm, $V_{valve} = 80$ pL), we estimated a ΔP of ~207 kPa to obtain $k_{system} = 2.7$ Pa. From this we determined the limiting pumping frequency as a function of viscosity, as plotted in Fig. 6. The curve defined by eqn (22) provides an upper bound on the range of pumping frequencies and viscosities for which accurate metering based on incremental increases in the volumetric flow rate can be accomplished, thus defining an "accurate metering window." Beyond this window the relation between the frequency and the volumetric flow rate is unclear, hampering accurate metering. Note that this analysis assumes that the channel or chamber into which the fluid is being pumped is rigid, thus transient effects can be ignored.

In their work, Hansen and coworkers reported that metering of a viscous fluid ($\eta \approx 0.4$ Pa s) could not be accomplished at a pumping rate of 10 Hz, whereas accurate metering could be done at a slower rate of 5 Hz. If we examine these two points graphically, we observe that the faster pumping rate of 10 Hz falls outside of the metering window (Fig. 6, ◇) whereas adjusting the pumping rate to 5 Hz shifts the condition so that it falls within the accurate metering window (Fig. 6, ◆). In other words, the simple approach, based on eqn (22), to indicate what ranges of operational parameters for a given system will allow for precise metering that we report here is able to accurately describe these experimentally observed data.

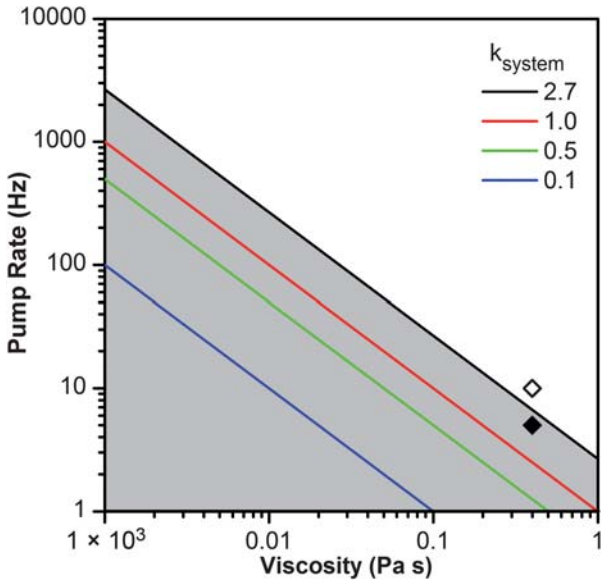

Fig. 6 Pump rate curves for peristaltic metering systems characterized by different values of k_{system}. These curves indicate the upper bound of an "accurate metering window." The black curve represents the system described by Hansen *et al.* with $k_{system} = 2.7$ Pa.[24] The associated metering window is highlighted in grey. Two points are shown, corresponding to the limiting case of 10 Hz (◇) which could not accurately meter a fluid with a viscosity of 0.4 Pa s, and 5 Hz (◆) which falls within the accurate metering window.

The case of a deforming channel. The fluid metering described above assumes that the channel or chamber into which the fluid is being pumped is rigid and that transient effects do not need to be taken into account. To examine the extent to which the initial transient can affect metering let us now consider the metering example from Hansen and coworkers[24] taking channel deformation into account. We assume here that $\beta = 1$ and that the timescale for actuation of the peristaltic pump is much faster than the timescale for channel deformation such that the discrete nature of peristaltic pump actuation can be neglected. Given the value of β, the analysis regarding the effect of channel deformation on viscous flow provided in Section 2.2 allows us to determine a variety of parameters for our system. For this metering example, the most important parameters are the steady-state volumetric flow rate, the lag time, and the lag volume. As was mentioned previously (Section 2.2.1), for a value of $\beta = 1$ the volumetric flow rate resulting from the deformed channel is 375% higher than the corresponding flow rate expected for a rigid channel. Thus if we perform the limiting pumping rate analysis from eqn (22) we observe that the deformation of the channel reduces the resistance to flow and thus allows the system to operate at a faster steady-state pumping rate than in the limit of the rigid case. In fact, for the same viscous fluid ($\eta \approx 0.4$ Pa s), we predict a maximum pumping rate of 25 Hz, a 5× increase.

The lag time and lag volume are also very important when taking the initial transient of a metering operation into account. For a system with $\beta = 1$, we use Fig. 4c to read off normalized values for these two parameters with respect to a rigid system ($V_{lagss}/V_{rigid} = 0.254$ and $\tau_{lagss}/\tau_{rigid} = 0.0679$). While the values of these normalized parameters are applicable to any system, the

Table 2 Scaling relationships for the lag volume (V_{lag}) and lag time (t_{lag}) associated with the initial transient resulting from channel deformation. These results were developed from the definitions for V_{rigid} and τ_{rigid}

Parameter	Lag volume	Lag time
w	$V_{lag} \approx w$	No effect
h	$V_{lag} \approx h$	$t_{lag} \approx 1/h^2$
L	$V_{lag} \approx L$	$t_{lag} \approx L^2$
ΔP	No effect	$t_{lag} \approx 1/\Delta P$
η	No effect	$t_{lag} \approx \eta$

actual dimensional values for the lag time and volume will depend on the system parameters involved in the normalization variables V_{rigid} and τ_{rigid}.

$$V_{rigid} = whL \tag{23}$$

$$\tau_{rigid} = \frac{V_{rigid}}{\dot{V}_{rigid}} = \frac{12\eta L^2}{h^2 \Delta P} \tag{24}$$

As can be seen in eqn (23) and (24), V_{rigid} scales linearly with the channel length L, whereas τ_{rigid} scales with the length squared. If we consider two channels where one is twice the length of the other and analyze the lag behavior associated with the initial transient we will see a significant difference between the two channels. The lag volume for the longer channel will be twice that of the shorter one while the lag time will be four times longer. A summary of these scaling relationships is given in Table 2.

Let us now consider the effects of this lag period on the metering example from Hansen and coworkers. For this system the accuracy of metering was taken to be equal to the volume pumped by a single cycle of the peristaltic pump, 80 pL. However, we determined a lag volume of 0.863 nL which corresponds to nearly 11 cycles of the pump. While the magnitude of this lag volume depends upon the channel geometry as shown in Table 2, it is important to note the potentially significant error in the volume of fluid metered that can result from channel deformation.

4. Conclusions

In summary, we have derived key equations for the actuation of microfluidic pneumatic valves and pressure-driven viscous flow in both rigid and deforming microfluidic channels at steady-state and unsteady conditions. We translated these mathematical expressions into a series of scaling relationships which can be used in the design, construction, and operation of microfluidic devices. Here we focused on pumping and precise metering. We then applied these design rules to two specific tasks: (i) the design of a microfluidic device to mix highly viscous fluids and (ii) the precise metering of fluids over a range of viscosities using an on-chip pneumatic peristaltic pump.

The analysis performed here focused on Newtonian fluids to clearly lay out the various scaling relationships that exist. However, similar rules can also be developed for non-Newtonian fluids. The two most commonly considered types of non-Newtonian fluid behavior are shear thickening and shear thinning, related to how the fluid reacts to different shear stresses. At a single flow condition, a non-Newtonian fluid can be described by an apparent viscosity, which can be used with the design equations developed here. Additional non-Newtonian behaviors such as viscoelasticity are characterized most importantly by a characteristic timescale. In the case of a viscoelastic fluid, actions that occur faster than this characteristic timescale for relaxation cause the material to respond elastically rather than as a viscous fluid. Thus by operating a device at a timescale longer than this relaxation time the non-Newtonian behavior will be negligible and the equations derived here for steady and unsteady flow of viscous fluids in microfluidic channels will still apply.

The design rules in this work will aid the design of microfluidic systems that involve a significant challenge, such as the need to handle high fluid viscosities or the need to meter fluids precisely. Furthermore, the results in this work for the first time quantify the transient effects that deforming channels have on the performance of microfluidic systems. This analysis will enable the design of devices whereby transient deformation effects can be minimized to a level that is acceptable for the intended application or where the transient effects can be accurately accounted for.

Acknowledgements

This work was funded by NIH (R01 GM086727) and a NIH Kirschstein Predoctoral Fellowship from the National Institute of Biomedical Imaging and Bioengineering (F31 EB008330). We thank Ashlee N. Ford for her assistance.

References

1 R. Pal, M. Yang, R. Lin, B. N. Johnson, N. Srivastava, S. Z. Razzacki, K. J. Chomistek, D. C. Heldsinger, R. M. Haque, V. M. Ugaz, P. K. Thwar, Z. Chen, K. Alfano, M. B. Yim, M. Krishnan, A. O. Fuller, R. G. Larson, D. T. Burke and M. A. Burns, *Lab Chip*, 2005, **5**, 1024–1032.
2 S. L. Perry, G. W. Roberts, J. D. Tice, R. B. Gennis and P. J. A. Kenis, *Cryst. Growth Des.*, 2009, **9**, 2566–2569.
3 R. C. R. Wootton and A. J. deMello, *Chem. Commun.*, 2004, 266–267.
4 R. S. Jayashree, L. Gancs, E. R. Choban, A. Primak, D. Natarajan, L. J. Markoski and P. J. A. Kenis, *J. Am. Chem. Soc.*, 2005, **127**, 16758–16759.
5 Y. N. Xia and G. M. Whitesides, *Angew. Chem., Int. Ed.*, 1998, **37**, 551–575.
6 J. A. Rogers and R. G. Nuzzo, *Mater. Today (Oxford, U. K.)*, 2005, **8**, 50–56.
7 T. Gervais, J. El-Ali, A. Gunther and K. F. Jensen, *Lab Chip*, 2006, **6**, 500–507.
8 J. C. Lötters, W. Olthuis, P. H. Veltink and P. Bergveld, *J. Micromech. Microeng.*, 1997, **7**, 145–147.
9 M. A. Unger, H. P. Chou, T. Thorsen, A. Scherer and S. R. Quake, *Science*, 2000, **288**, 113–116.
10 B. R. Schudel, C. J. Choi, B. T. Cunningham and P. J. A. Kenis, *Lab Chip*, 2009, **9**, 1676–1680.
11 H. P. Chou, M. A. Unger and S. R. Quake, *Biomed. Microdevices*, 2001, **3**, 323–330.
12 V. Studer, G. Hang, A. Pandolfi, M. Ortiz, W. F. Anderson and S. R. Quake, *J. Appl. Phys.*, 2004, **95**, 393–398.
13 E. P. Kartalov, A. Scherer, S. R. Quake, C. R. Taylor and W. F. Anderson, *J. Appl. Phys.*, 2007, **101**, 064505.
14 J. Goulpeau, D. Trouchet, A. Ajdari and P. Tabeling, *J. Appl. Phys.*, 2005, **98**, 044914–044919.
15 L. Li, Q. Fu, C. Kors, L. Stewart, P. Nollert, P. Laible and R. Ismagilov, *Microfluid. Nanofluid.*, 2009, **8**, 789–798.
16 J. C. McDonald, D. C. Duffy, J. R. Anderson, D. T. Chiu, H. K. Wu, O. J. A. Schueller and G. M. Whitesides, *Electrophoresis*, 2000, **21**, 27–40.

17 M. E. Vlachopoulou, A. Tserepi, P. Pavli, P. Argitis, M. Sanopoulou and K. Misiakos, *J. Micromech. Microeng.*, 2009, **19**, 015007.
18 R. B. Bird, W. E. Stewart and E. N. Lightfoot, *Transport Phenomena*, John Wiley & Sons, New York, 1960.
19 B. S. Hardy, K. Uechi, J. Zhen and H. P. Kavehpour, *Lab Chip*, 2009, **9**, 935–938.
20 M. A. Holden, S. Kumar, A. Beskok and P. S. Cremer, *J. Micromech. Microeng.*, 2003, **13**, 412–418.
21 S. Timoshenko, *Strength of Materials, Part II: Advanced Theory and Problems*, D. Van Nostrand Company, Inc., Princeton, NJ, 1955.
22 A. E. H. Love, *A Treatise on the Mathematical Theory of Elasticity*, Cambridge University Press, Cambridge, 1934.
23 *MATLAB version 7.6.0.234*, Mathworks Inc., Natick, MA, 2008.
24 C. L. Hansen, M. O. A. Sommer and S. R. Quake, *Proc. Natl. Acad. Sci. U. S. A.*, 2004, **101**, 14431–14436.
25 T. M. Squires and S. R. Quake, *Rev. Mod. Phys.*, 2005, **77**, 977–1026.
26 A. D. Stroock, S. K. W. Dertinger, A. Ajdari, I. Mezic, H. A. Stone and G. M. Whitesides, *Science*, 2002, **295**, 647–651.
27 A. D. Stroock, S. K. Dertinger, G. M. Whitesides and A. Ajdari, *Anal. Chem.*, 2002, **74**, 5306–5312.
28 J. M. Ottino, *The kinematics of mixing: stretching, chaos, and transport*, Cambridge University Press, Cambridge, 1989.
29 M. Caffrey, *Annu. Rev. Biophys.*, 2009, **38**, 29–51.

